





# Effect of excessive Cs and O on activation of GaAs(100) surface: From experiment to theory

Cite as: J. Appl. Phys. **128**, 173103 (2020); <https://doi.org/10.1063/5.0028042>

Submitted: 02 September 2020 . Accepted: 20 October 2020 . Published Online: 05 November 2020

 Yijun Zhang,  Kaimin Zhang,  Shiman Li,  Shan Li, Yunsheng Qian, Feng Shi, Gangcheng Jiao, Zhuang Miao, Yiliang Guo, and Yugang Zeng



View Online



Export Citation



CrossMark

## ARTICLES YOU MAY BE INTERESTED IN

Use of carrier injection engineering to increase the light intensity of a polycrystalline silicon avalanche mode light-emitting device

Journal of Applied Physics **128**, 173104 (2020); <https://doi.org/10.1063/5.0020113>

Evolution of the electrical characteristics of Cu(In,Ga)Se<sub>2</sub> devices with sodium content

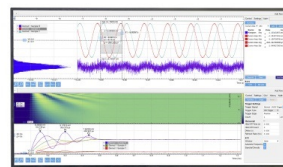
Journal of Applied Physics **128**, 173102 (2020); <https://doi.org/10.1063/5.0025183>

In situ investigation of hot-electron-induced Suzuki–Miyaura reaction by surface-enhanced Raman spectroscopy

Journal of Applied Physics **128**, 173105 (2020); <https://doi.org/10.1063/5.0023623>

## Challenge us.

What are your needs for periodic signal detection?



Zurich  
Instruments

# Effect of excessive Cs and O on activation of GaAs (100) surface: From experiment to theory

Cite as: J. Appl. Phys. 128, 173103 (2020); doi: 10.1063/5.0028042

Submitted: 2 September 2020 · Accepted: 20 October 2020 ·

Published Online: 5 November 2020



Yijun Zhang,<sup>1,a)</sup> Kaimin Zhang,<sup>1</sup> Shiman Li,<sup>1</sup> Shan Li,<sup>1</sup> Yunsheng Qian,<sup>1</sup> Feng Shi,<sup>2</sup> Gangcheng Jiao,<sup>2</sup> Zhuang Miao,<sup>2</sup> Yiliang Guo,<sup>3</sup> and Yugang Zeng<sup>4</sup>

## AFFILIATIONS

<sup>1</sup>School of Electronic and Optical Engineering, Nanjing University of Science and Technology, Nanjing 210094, China

<sup>2</sup>Science and Technology on Low-Light-Level Night Vision Laboratory, Xi'an 710065, China

<sup>3</sup>North Night Vision Technology Co., Ltd, Nanjing 211106, China

<sup>4</sup>Changchun Institute of Optics, Fine Mechanics and Physics, Chinese Academy of Sciences, Changchun 130033, China

<sup>a)</sup>Author to whom correspondence should be addressed: zhangyijun423@126.com

## ABSTRACT

The surface Cs–O activation process directly determines quantum efficiency and stability of negative-electron-affinity photocathodes. To investigate the effects of excessive Cs and O supply on activation and to explore a more effective Cs–O activation recipe, Cs–O activation experiments of GaAs(100) photocathodes are carried out based on the current-driven solid Cs and O dispensers. By a comparison of differences in activation photocurrent, quantum efficiency, and photocurrent decay, it is found that the recipe of excessive O and non-excessive Cs is not suitable for activating GaAs photocathodes, while the recipe of continuous and completely excessive Cs along with intermittent and non-excessive O can achieve the most excellent photoemission performance, including the highest quantum efficiency in the long-wave threshold region and best stability under intense light irradiation after activation. Furthermore, this improved activation recipe with the least Cs–O alternating cycles is easier to operate. Combined with density functional calculations and dipole layer model, it is found that the activation recipe of completely excessive Cs and non-excessive O can form effective dipoles to the greatest extent, and avoid the direct interaction between As atoms and O atoms to form As–O–Ga oxides on the GaAs(100) reconstructed surface.

Published under license by AIP Publishing. <https://doi.org/10.1063/5.0028042>

## I. INTRODUCTION

Due to the excellent properties including high quantum efficiency, large current density, low dark emission, high polarizability, and centralized electron energy distribution, negative-electron-affinity (NEA) GaAs photocathodes have been widely used in many fields such as high-performance low-light image intensifiers, spin-polarized electron sources, low-voltage scanning electron microscopes, and photon-enhanced thermionic energy converters.<sup>1–4</sup> In practical applications, quantum efficiency and stability are important indicators to evaluate the performance of the NEA GaAs photocathode, so improving the quantum efficiency and emission stability of GaAs photocathodes at the same time has been the focus in the field of cathode R&D so far.<sup>5–8</sup>

The quantum efficiency and stability of GaAs photocathodes are closely related to the cesium (Cs)–oxygen (O) activation process.<sup>9–11</sup> Nowadays, Cs–O activation recipes of GaAs photocathodes can be mainly divided into two types: yo–yo activation recipe with an

alternately intermittent Cs supply and O supply, and co-deposition activation recipe with a continuous Cs supply and intermittent O supply.<sup>12–14</sup> Compared with the traditional yo–yo activation recipe, the co-deposition activation recipe has been gradually preferred to activate GaAs photocathodes due to the virtues of easier operation and equally excellent photoemission performance.<sup>15</sup> Based on the Cs–O co-deposition recipe, Miao *et al.* studied the effects of different ratios of Cs/O on the performance of GaAs photocathodes and found that more Cs flux could contribute to the enhancement of cathode stability.<sup>16</sup> Togawa *et al.* proposed an improved yo–yo activation recipe, named as “Nagoya activation recipe,” which can improve the quantum efficiency of cathodes through maximizing the Cs flux.<sup>17</sup> Based on the co-deposition activation recipe, Zhang *et al.* realized the computer-controlled activation of GaAs photocathodes using the solid oxygen dispensers instead of gaseous oxygen, so as to achieve the desired symmetry of the photocurrent curve shape.<sup>11</sup> Although the activation process of GaAs photocathodes has been extensively

studied, the effects of excessive Cs flux and excessive O flux on the cathode performance during the Cs–O co-deposition activation process require further experimental verification. Meanwhile, the problem of frequent switch of a Cs or O source in the process of the whole Cs–O activation process is not conducive to the implementation of computer-controlled automatic activation, especially when the gaseous oxygen is controlled by a leak valve.<sup>18</sup> Therefore, the activation process of GaAs photocathodes still needs further optimization.

In this paper, by using the solid Cs and O dispensers and the co-deposition activation recipe, the effect of excessive Cs and O supply on the activation of the reflection-mode GaAs photocathode is investigated by experiments in terms of activating photocurrent, quantum efficiency, and photocurrent decay. Inspired from the “Nagoya activation recipe,” an improved activation recipe was proposed, which can achieve higher long-wave quantum efficiency and better emission stability, with fewer alternating cycles and an easier operating nature at the same time. Combined with the experimental results, first-principles calculations based on the density functional theory (DFT) were used to qualitatively explain the adsorption of excessive Cs and non-excessive O on the GaAs(100) reconstructed surface.

## II. EXPERIMENTAL

The reflection-mode GaAs cathode samples used in the activation experiments were all cleaved from the same 2-in.-diameter GaAs wafer grown by metalorganic vapor phase epitaxy, and the size was  $11 \times 11 \text{ mm}^2$ . The epilayers including a  $0.5\text{-}\mu\text{m}$ -thick p-type  $\text{Ga}_{1-x}\text{Al}_x\text{As}$  buffer layer and a  $1.0\text{-}\mu\text{m}$ -thick p-type GaAs emission layer were grown on a low-defect GaAs(100) substrate. In the  $\text{Ga}_{1-x}\text{Al}_x\text{As}$  buffer layer, the zinc-doping concentration was  $1 \times 10^{19} \text{ cm}^{-3}$  and the Al composition varied linearly from 0.9 to 0, while in the GaAs emission layer, the zinc-doping concentration changed from  $1 \times 10^{19} \text{ cm}^{-3}$  reduced to  $1 \times 10^{18} \text{ cm}^{-3}$  in a quasi-exponential form.<sup>19</sup> The cleaved samples were first degreased in the acetone and ethanol by ultrasonic cleaning, and then etched with HF acid solution followed by the HCl-isopropanol solution, which has more advantages in removing oxides and carbon contaminations.<sup>20</sup> Before loaded into the vacuum, the wet chemical etched samples were rinsed in de-ionized water and dried with nitrogen. After that, the samples were transferred to the preparation chamber with a base pressure of of  $1 \times 10^{-7} \text{ Pa}$  and were annealed at  $450^\circ\text{C}$  for 10 min to obtain the As-stabilized  $(2 \times 4)$  reconstruction surface.<sup>21</sup> After the sample temperature dropped to room temperature, Cs–O activation was performed. The schematic diagram of the Cs–O activation setup is shown in Fig. 1. During the activation process, a 12 V/100 W halogen lamp via the optical fiber was used as the electron-excited light source, and the commercial solid Cs dispensers from SAES Getters and self-developed solid O dispensers packaged in nickel containers were used as the activation sources.<sup>11</sup> Through a multi-information online measurement and control system, the flux of the Cs source and O source could be adjusted by controlling the applied direct current. Meanwhile, photoelectrons generated by the illuminating light were collected by the ring anode under a 200 V biased voltage, and the photocurrent changes were recorded online by the computer.

In order to investigate the effects of excessive Cs and O supply on the activation performance of GaAs photocathode during the

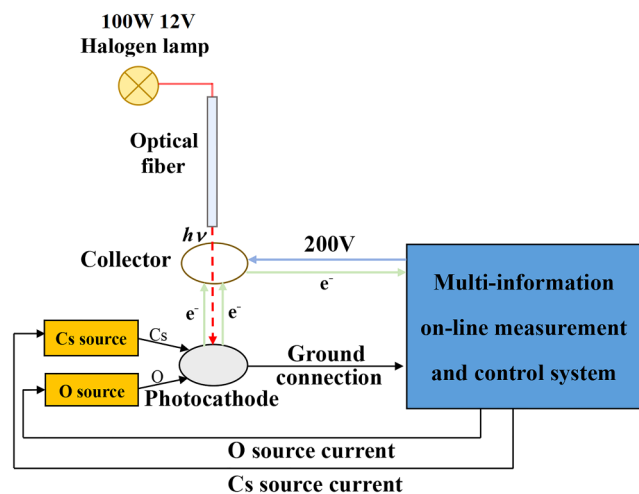


FIG. 1. Schematic diagram of the Cs–O activation setup.

activation process, four GaAs cathode samples numbered by sample 1 to sample 4, cleaved from the same epitaxial wafer, were activated by four different Cs–O activation recipes. The four groups of Cs–O activation experiments were labeled as A, B, C, and D. In all activation experiments, the Cs source current was 4.0 A and O source current was 1.7 A. The processes of the activation experiments corresponding to samples 1, 2, 3, and 4 were as follows:

### A. Activation experiment A

When the photocurrent reached the peak for the first time, the O source was introduced, while the Cs source was still continued. After that, a new peak of the photocurrent appeared and when the photocurrent dropped to 85% of the new peak due to the excessive supply of O flux, the O source was stopped. When the photocurrent rose to another peak again caused by the Cs flux, the O source was introduced again. This procedure was repeated until the photocurrent peak no longer increased.

### B. Activation experiment B

After the photocurrent reached the peak for the first time and then dropped to 85% of the peak due to the excessive supply of Cs flux, the O source was introduced, while the Cs source was still continued. Until a new peak of photocurrent appeared, the O source was stopped. Then, when the photocurrent rose to another new peak and immediately dropped to 85% of the new peak, the O source was introduced again. This procedure was also repeated until the photocurrent peak no longer increased.

### C. Activation experiment C

The “Nagoya activation recipe” was used.<sup>17</sup> After the photocurrent reached the peak for the first time and then dropped to a certain minimum value with a very slow decay rate due to the completely excessive supply of the Cs flux, the Cs source was

stopped and the O source was introduced. When the photocurrent reached a new peak, the O source was stopped and the Cs source was introduced to drop the photocurrent again. This procedure was also repeated until the photocurrent peak no longer increased.

#### D. Activation experiment D

Differing from the “Nagoya activation recipe,” the Cs source was supplied all along. After the photocurrent reached the peak for the first time and then dropped to a certain minimum value with a very slow decay rate due to the completely excessive supply of the Cs flux, and the O source was introduced while the Cs source was still continued. When the photocurrent reached a new peak, the O source was stopped and the photocurrent dropped to the certain

minimum value again. This procedure was also repeated until the photocurrent peak no longer increased.

After Cs–O activation, the quantum efficiency curves and the photocurrent decay curves were tested by the multi-information online measurement and control system. In the photocurrent decay process after activation, the samples were still illuminated with the same 12/100 W white halogen light source and the vacuum pressure was around  $2 \times 10^{-7}$  Pa.

### III. RESULTS

#### A. Activation photocurrent comparison

In the four groups of Cs–O activation experiments, the Cs source current, O source current, and photocurrent were recorded online, as shown in Fig. 2. In the Cs–O activation process, the

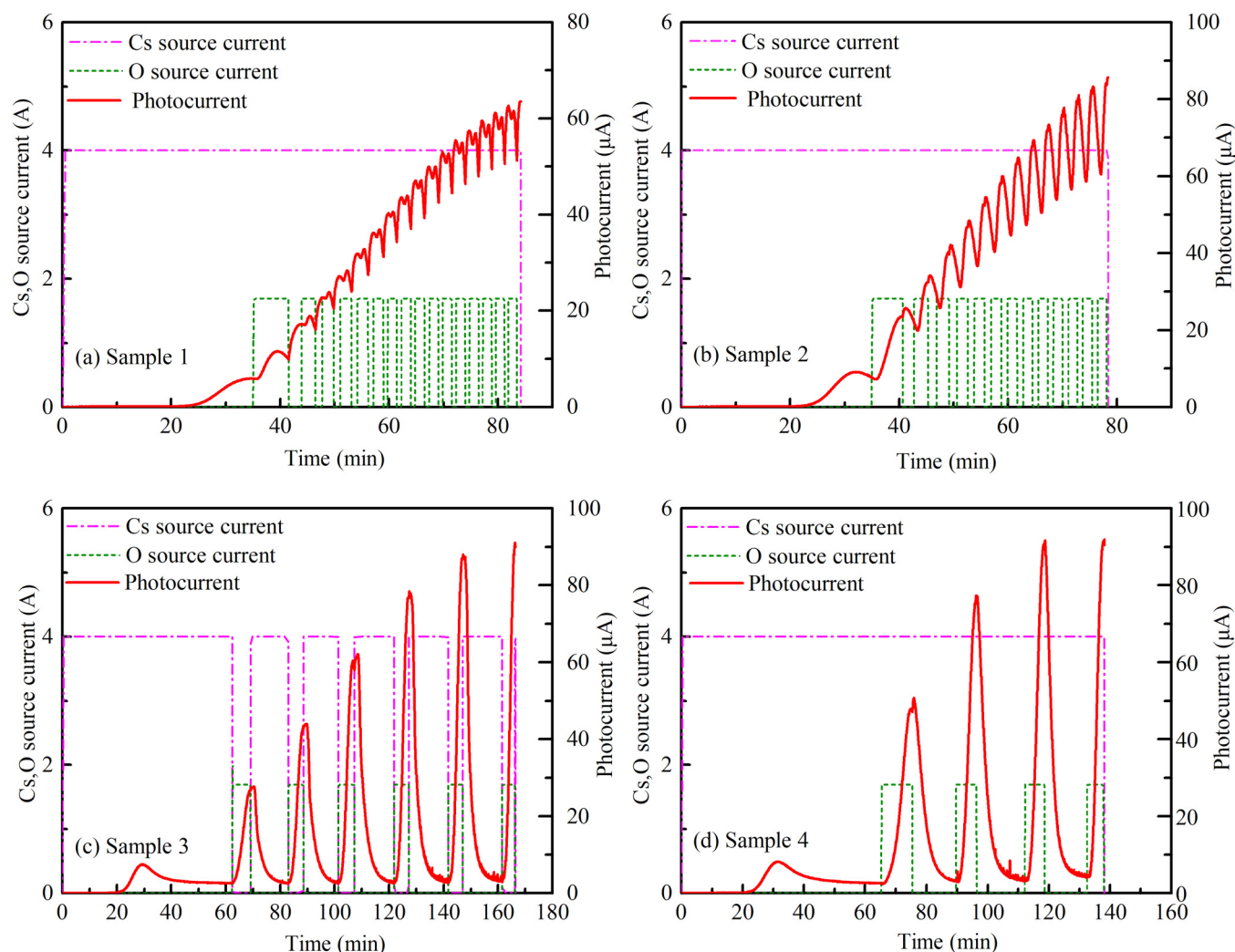


**FIG. 2.** Cs–O activation processes of the four GaAs cathode samples corresponding to (a) activation experiment A, (b) activation experiment B, (c) activation experiment C, and (d) activation experiment D, respectively.

changes in the vacuum pressure in the Cs–O activation process for the four GaAs cathode samples are given in Fig. S1 in the [supplementary material](#). For experiments A and B, the co-deposition activation recipe was based on the continuous Cs and intermittent O. The difference between them lies in the O supply. In experiment A, the Cs supply is non-excessive, while the O supply is excessive. In experiment B, the Cs supply is excessive, while the O supply is non-excessive. From [Figs. 2\(a\) and 2\(b\)](#), it is seen that, according to the two Cs–O activation processes, the Cs–O alternation time is relatively longer in the early stage, and with the number of alternating cycles increases, the Cs–O alternating cycle time gets shortened. During the alternating activation process, it takes a period of time for the photocurrent to rise after the O source is introduced, and with the decrease in the Cs–O alternating cycle time, this phenomenon becomes more obvious. The reason is that the release of oxygen molecules requires a certain warm-up time after the current-driven O source is turned on. By comparison of the activation results in [Figs. 2\(a\) and 2\(b\)](#), it is found that the final photocurrent of activation experiment B with excessive Cs is much higher than that of activation experiment A with excessive O. Although activation experiment A has more alternating cycles, the increase in the photocurrent after Cs–O alternating activation is not so high. For activation experiment A, the photocurrent exhibits a large increase after the O source is introduced for the first time, while in the following alternating activation process, the photocurrent only increases when the O source is stopped and Cs is supplied alone. When both Cs and O sources are supplied, the photocurrent increases slightly and then decreases quickly. It is noted that the case of photocurrent change in activation experiment B is completely different. After each time the O source is turned on, the photocurrent increases significantly and increases slightly when the O source is stopped and only Cs flux is supplied.

Two groups of activation experiments C and D are designed to investigate whether excessive Cs can be advantageous to the Cs–O activation. The activation results of the traditional “Nagoya activation recipe” are shown in [Fig. 2\(c\)](#). The activation photocurrent of activation experiment C is higher than those of activation experiments A and B. The activation recipe of experiment D is improved on the basis of activation experiment C. In the activation experiment D, Cs supply is continuous, and the O supply is intermittent. This activation recipe obtains a higher final photocurrent as same as that of activation experiment C, and the number of activation cycles is much less than activation experiments A and B. Although activation experiments C and D have less Cs–O alternating cycles, the photocurrent decay time and average alternating

cycle time is extended each time when Cs is excessive, and the total activation time of activation experiments C and D is longer. From [Figs. 2\(c\) and 2\(d\)](#), it is found that when the Cs source is completely excessive, the activation with the continuous Cs flux and intermittent O flux can be obtained the same high photocurrent as well as the “Nagoya activation recipe.” Compared with activation experiment C, the activation experiment D has the higher photocurrent peak after the first O introduction and fewer Cs–O alternate cycles, thereby, the total activation time is shortened. Besides, as for the activation recipe D, only the O source needs to be switched while the Cs source is kept on, so this improved activation recipe is easier to operate.

The parameters of the Cs–O activation process corresponding to the four GaAs cathode samples are listed in [Table I](#). It is seen that, for the four samples, the photocurrent starts to increase at about 20 min after the initial Cs supply, and the time when the photocurrent reaches the first Cs peak is nearly coincident, indicating that the Cs deposition rates and amounts in the initial Cs activation experiments are approximately the same. The less Cs–O alternating cycles in activation experiments C and D for samples 3 and 4 indicate that a completely excessive Cs flux during activation can be applied to reduce the number of alternating cycles, and the average Cs–O alternating cycle time is also extended. By comparing the final photocurrent, it is found that sample 1 in activation experiment A with non-excessive Cs flux and excessive O flux has the lowest photocurrent, and sample 4 in activation experiment D in which the Cs flux is continuous and completely excessive has the highest photocurrent. Compared with sample 3, sample 4 has less activation alternating cycles and shorter total activation time. Therefore, the activation recipe D of continuous and completely excessive Cs along with intermittent O is more conducive to achieve high photocurrent.

## B. Quantum efficiency comparison

Quantum efficiency is an important parameter for evaluating the photoresponse capability of the photocathode under the irradiation in the wavelength range of interest. Through the multi-information online measurement and control system, the quantum efficiency curves of the four Cs–O activated GaAs photocathode samples in the region of 400–1000 nm were tested *in situ*, which are shown in [Fig. 3](#).

From the cutoff wavelengths, it is known that the surface of the four GaAs cathode samples shows the NEA state through Cs–O activation. Sample 4 in activation experiment D has the highest spectral responsivity, while sample 1 in activation experiment A

**TABLE I.** Cs–O activation process parameters of the four GaAs cathode samples.

Sample	First Cs peak time (min)	First Cs peak photocurrent ( $\mu\text{A}$ )	Cs–O alternating cycles	Average alternating cycle time (min)	Final photocurrent ( $\mu\text{A}$ )	Total activation time (min)
1	34	6.0	16	2.9	63.5	84
2	33	8.0	13	3.1	85.6	78
3	30	7.4	6	19.0	90.3	166
4	32	8.1	4	20.0	91.5	138

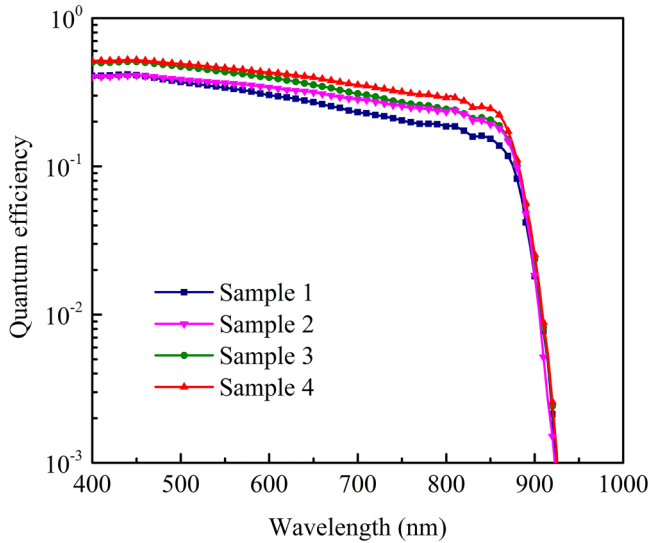


FIG. 3. Quantum efficiency curves of the four GaAs cathode samples.

has the lowest spectral responsivity. By comparison of quantum efficiency curves between samples 1 and 2, it is found that sample 2 activated with excessive Cs flux and non-excessive O flux can obtain a higher quantum efficiency in the long-wave response region than sample 1 activated with non-excessive Cs flux and excessive O flux. For samples 3 and 4 both with complete excessive Cs flux activation, the quantum efficiency of sample 4 with continuous Cs and intermittent O activation is higher in the long-wave response region than that of sample 3 with alternately intermittent Cs–O activation. Therefore, it is inferred that, through the excessive Cs flux activation, the surface barrier of GaAs photocathode can be lowered to be more favorable for the escape of low-energy electrons excited by long-wave light. In a word, the activation recipe of continuously and completely excessive Cs flux can effectively improve the quantum efficiency of GaAs photocathodes, especially in the long-wave threshold region.

### C. Stability comparison

The photocurrent decay under intense white light irradiation was executed immediately after the quantum efficiency test, and the results are shown in Fig. 4(a). Meanwhile, the changes of vacuum pressure in the decay process for the four cathode samples are seen in Fig. S2 in the [supplementary material](#). Because of the poor vacuum pressure at the level of  $10^{-7}$  Pa and the intense white light irradiation of 100 lx, the photocurrent decay rates of the four cathode samples are relatively fast. Usually, the decay of photocurrent or quantum efficiency at room temperature can be fitted by means of single exponential lifetime analysis.<sup>22</sup> However, the simulated curve in this simple form is not consistent with our experimental data. In this case, two forms of fitting formula regarding the photocurrent decay under intense white light irradiation are

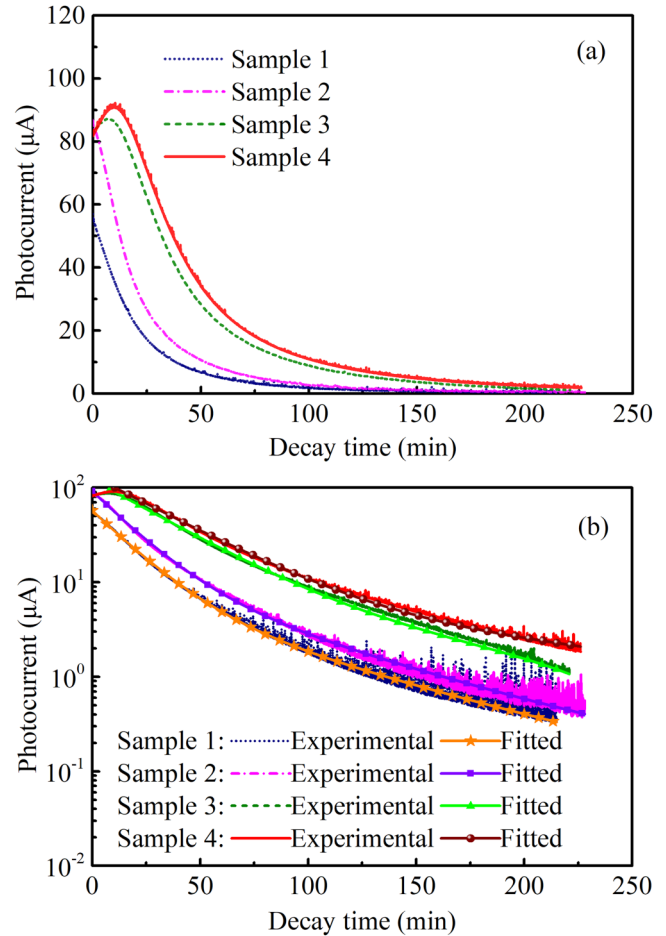


FIG. 4. Stability test results of the four GaAs cathode samples. (a) Linear ordinate and (b) logarithmic ordinate.

proposed empirically, which are expressed as

$$I(t) = I_1 e^{-at} + I_2 e^{-bt} + I_3, \quad (1)$$

$$I(t) = I_1 e^{-at} - ct^2 + I_3, \quad (2)$$

where  $I_1$  and  $I_2$  are defined as the dominant photocurrent and secondary photocurrent, respectively,  $I_3$  is the relatively stable photocurrent after decay,  $a$  is defined as the dominant decay coefficient, and  $b$  and  $c$  are defined as the secondary decay coefficient. Note that no single fitting formula can be applicable to the four samples at the same time, and it is found that Eq. (1) is applicable to samples 1 and 2, while Eq. (2) is applicable to samples 3 and 4. The reason for the difference in the fitting formula is not clear, but it should be related to the adsorption of Cs on the surface. In Eqs. (1) and (2), the smaller the decay coefficient, the better the emission stability. In addition, the dominant decay coefficient  $a$

**TABLE II.** Fitted parameters of the photocurrent decay curves for the four GaAs cathode samples.

Sample	$I_1$ ( $\mu\text{A}$ )	$I_2$ ( $\mu\text{A}$ )	$I_3$ ( $\mu\text{A}$ )	$a$	$b$	$c$
1	50.2662	7.0898	0.0500	0.0541	0.0152	N/A
2	80.1761	11.8661	0.0800	0.0541	0.0158	N/A
3	93.6352	N/A	2.7101	0.0297	N/A	$4.0 \times 10^{-5}$
4	97.4396	N/A	2.8632	0.0277	N/A	$2.2 \times 10^{-5}$

plays a more important role than secondary decay coefficient  $b$  and  $c$ .

By comparison of photocurrent decay curves, it is seen that, under the same environmental conditions, samples 3 and 4 have better emission stability, while samples 1 and 2 have worse emission stability. In addition, it is worth noting that the photocurrent of samples 1 and 2 in experiments A and B decays from the beginning, while the photocurrent of samples 3 and 4 in experiments C and D first rises to the another peak value, then decays with time. Because Cs sources are both continuously supplied in activation experiments A and B, the advantage in emission stability of sample 2 with excessive Cs supply and non-excessive O supply is not obvious. In activation experiments C and D, Cs supply is completely excessive, and the difference lies in whether the Cs source supply is continuous or not in the whole activation process. The experimental photocurrent decay curves of the four GaAs cathode samples are well fitted by using Eqs. (1) and (2), as shown in Fig. 4(b), wherein the ordinate scale is in the logarithmic form to highlight the fitting consistency. Besides, the first ten minutes of photocurrent increase for samples 3 and 4 are ignored for a better fit. The fitted parameters of the photocurrent decay curves for the four samples are listed in Table II. It is seen from Table II that the dominant decay coefficient  $a$  for samples 3 and 4 is approximately half of that for samples 1 and 2. Compared with sample 1, sample 2 has an equal dominant decay coefficient  $a$  and a slightly larger secondary decay coefficient  $b$ . Nevertheless, the inappreciable difference in secondary decay coefficient for samples 1 and 2 can be ignored. Among the four samples, sample 4 has the minimum dominant decay coefficient  $a$ , which means the best emission stability for sample 4. Compared with sample 3 with the intermittent Cs supply, sample 4 with the continuous Cs supply has a smaller dominant decay coefficient  $a$  and a smaller secondary decay coefficient  $c$ . Therefore, it can be inferred that the time of Cs overdose is vital to the cathode stability after activation. The excessive Cs flux is beneficial to the formation of a more stable Cs–O activation layer on the GaAs surface, and the orderly and robust surface dipoles can weaken the damage of vacuum residual gas on the surface and reduce the decay rate of cathode photoemission capability.

#### IV. DISCUSSION

The above experimental results demonstrate that the GaAs cathode sample activated with non-excessive Cs and excessive O has the lowest final photocurrent and near-infrared response, and the quickest photocurrent decay rate under intense white light

irradiation after activation, whereas the case of the GaAs cathode sample activated with completely excessive Cs and non-excessive O is quite different. This phenomenon indicates that the improved activation recipe can make the adsorbed Cs–O activation layer more stable and more effective to reduce surface work function. According to the double dipole layer model proposed by Su *et al.*,<sup>23</sup> the NEA surface of activated GaAs photocathode is formed by the formation of the GaAs–O–Cs dipole layer and  $\text{Cs}^+ \text{O}^{2-} \text{Cs}^+$  dipole layer. Therefore, the surface barrier of the GaAs cathode can have a blocking effect on the escape of low-energy photoelectrons excited by near-infrared photons, while the height and width of the surface barrier are closely related to the effective adsorption of Cs–O on the cathode surface. It can be inferred that the activation recipe with excessive O flux and non-excessive Cs flux can cause O atoms to interact with the GaAs surface to form more oxides, which will construct a higher and wider surface barrier to hinder the decrease of the work function. In order to confirm this conjecture, it is necessary to study the effect of different situations of Cs–O adsorption on the GaAs surface from the atomic level by first-principles calculation.

Considering that all cathode samples activated in the experiments are (100)-oriented p-type GaAs, and the GaAs(100)- $\beta_2(2 \times 4)$  reconstruction surface is the most stable and most concerned surface.<sup>24–29</sup> Besides, the As-stabilized GaAs(100)- $(2 \times 4)$  reconstruction surface was observed after treatment in HCl–isopropanol solution and subsequent annealing at  $410 \sim 480^\circ\text{C}$  in ultrahigh vacuum.<sup>21</sup> In this case, a seven-layer GaAs(100)- $\beta_2(2 \times 4)$  reconstruction surface model consisting of four layers of As atoms and three layers of Ga atoms was built, wherein there were 28 As atoms, 21 Ga atoms, and 1 Zn atom in the fourth layer substituted for 1 Ga atom as the p-type dopant. In this case, the doping ratio is 1/50, namely, the doping density is in the order of magnitude of  $10^{20} \text{ cm}^{-3}$ . In the surface structure, the reconstruction phase contains two As dimers in the top layer and one As dimer in the third layer. Besides, the pseudo-hydrogen atoms are situated at the bottom to saturate the dangling bonds. As for the GaAs(100)- $\beta_2(2 \times 4)$  reconstruction surface, researchers have found that As–O–Ga oxides from the bonding of one O atom, one As atom in the top As dimer, and one adjacent Ga atom with the dangling bond is more stable than As–O–As or As=O oxides from the bonding of one O atom and two dimer As atoms in the first layer or third layer.<sup>27,28</sup> In order to understand the mechanism of Cs adsorption, Cs–O adsorption and GaAs oxides on the surface properties, different absorption models, such as Cs adsorption, Cs–O adsorption, Cs-bonded O adsorption, 2Cs–O adsorption, and 2Cs adsorption on the clean GaAs(100)- $\beta_2(2 \times 4)$  reconstruction surface were built, as shown in Fig. 5, where Cs atoms and O atoms are all located nearby the As atoms in the top As dimer and adjacent Ga atoms with the dangling bond in the second layer. In Fig. 5(d), the stable As–O–Ga oxide from the bonding of one As atom in the top As dimer and one adjacent Ga atom with the dangling bond in the second layer was preferred as an example. By using the CASTEP software package, first-principles calculations based on DFT were performed on these models. In the calculations, the exchange correlation energy interaction was treated by the generalized-gradient-approximation (GGA) Perdew–Burke–Ernzerhof (PBE) functional, and the Broyden–Fletcher–Goldfarb–Shanno (BFGS) algorithm was used for geometry

## Top view

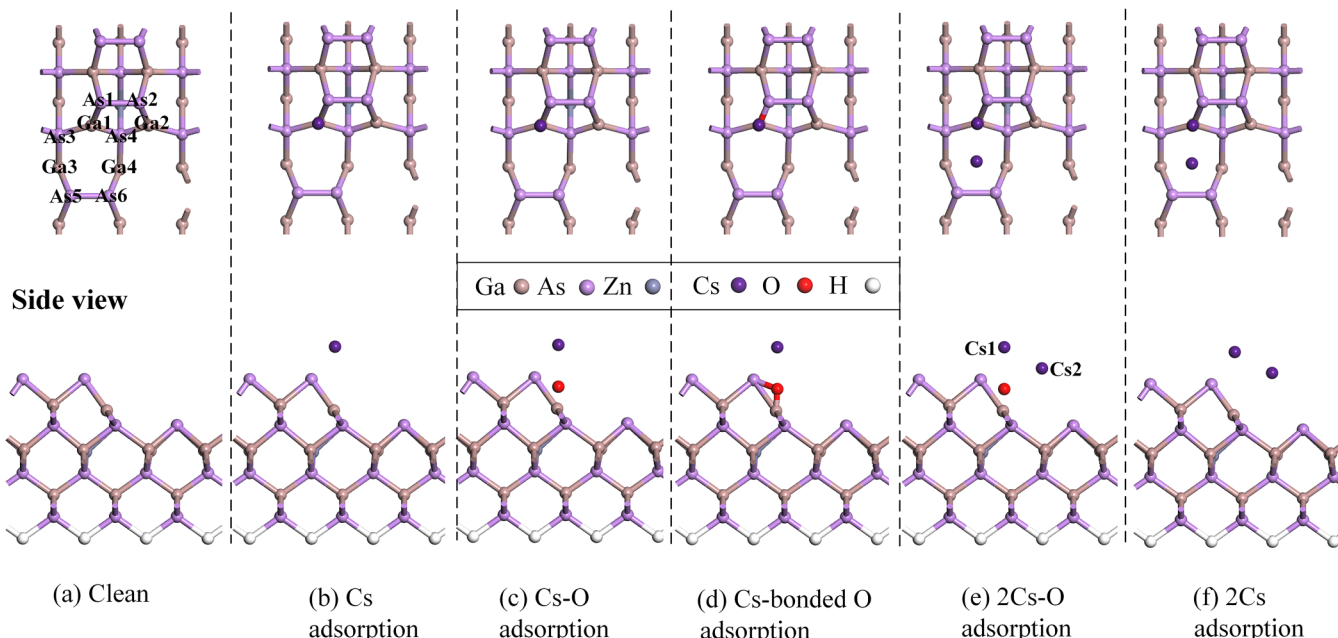


**FIG. 5.** Top and side views of the six surface models before geometry optimization corresponding to (a) clean, (b) Cs adsorption, (c) Cs–O adsorption, (d) Cs-bonded O adsorption, (e) 2Cs–O adsorption, and (f) 2Cs adsorption, respectively.

optimization. The ultra-soft pseudopotential plane wave cutoff energy of 400 eV and the convergence accuracy of  $2 \times 10^{-6}$  eV/atom were adopted, and the K-point mesh grid in the form of Monkhorst–Pack was set as  $6 \times 3 \times 1$ . In the optimization process, the top four layers above were allowed to fully relax and the remaining layers below were constrained and always fixed in the ideal position. The vacuum layer with a thickness of 15 Å was used to avoid mirror interaction between the two periodic slab surfaces.

The calculation results of work function corresponding to these six surface models are presented in Fig. 6. It can be seen that work function of the clean GaAs(100)- $\beta_2(2 \times 4)$  reconstruction surface is 4.7 eV. When one Cs atom is adsorbed on the surface, i.e., the Cs surface density is 0.78 atoms/nm<sup>2</sup>, the work function decreases due to the orbital electron transfer between Cs atom and surface As atoms. When one O atom locates below the Cs atom close to the Ga atom with a dangling bond in the second layer, the work function does not decrease; instead, it slightly increases to 3.86 eV. When the O atom below the Cs atom forms a bond with the As atom in the top As dimer and the adjacent Ga atom with the dangling bond, the surface work function further rises. If there are two Cs atoms above the O atom, the surface work function changes remarkably and drops to 2.9 eV, which could be related to the interaction of Cs atoms, O atoms, and surface Ga/As atoms. When only two Cs atoms are adsorbed on the surface, i.e., the Cs surface density is 1.56 atoms/nm<sup>2</sup>, the surface work function further decreases. This change in the surface work function indicates that surface Cs/O ratio has a significant effect on the emission ability of GaAs photocathodes.

Mulliken charge population analysis can reflect atomic charge distribution, charge transfer, and chemical property. Figure 7 gives the respective value of Mulliken charge population of atoms at different sites, where all the considered atoms marked as Ga1 ~ Ga4,

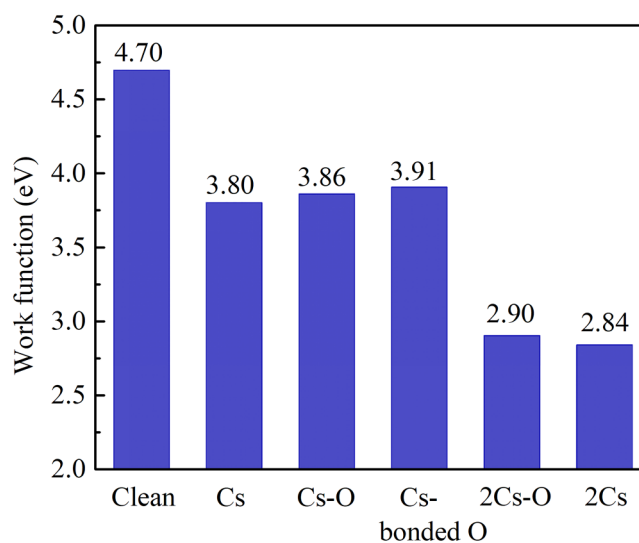


**FIG. 6.** Work function of the GaAs(100)- $\beta_2(2 \times 4)$  reconstruction surface with different adsorption models.

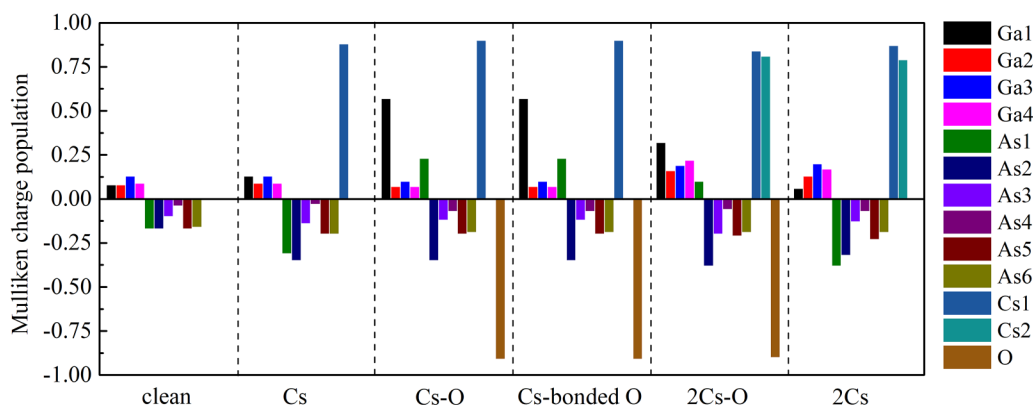


FIG. 7. Mulliken charge population of atoms at different sites on the GaAs(100)- $\beta_2(2 \times 4)$  reconstruction surface.

As1 ~ As6, Cs1, Cs2, and O are located on the GaAs(100)- $\beta_2(2 \times 4)$  reconstruction surface as shown in Fig. 5. A larger negative value indicates that more electrons are obtained, while a larger positive value indicates that more electrons are lost. As for the clean GaAs(100)- $\beta_2(2 \times 4)$  reconstruction surface, a Ga-As bond exists in the form of covalent bonds, and Ga atoms are positively charged, while As atoms are all negatively charged, because the electronegativity of As atoms is greater than that of Ga atoms. When one Cs atom marked as Cs1 is adsorbed at the position shown in Fig. 5(b), the positive charge population of Ga1 increases, and the absolute value of negative charge population of As1 and As2 increases more evidently, indicating that the adsorbed Cs atom prefers to interact with As1 and As2 in the top As dimers, and charge transfer occurs among them. When one O atom is adsorbed above the Ga1 atom as shown in Fig. 5(c), the charge population of O becomes negative, and the charge population of As1 adjacent to the O atom changes from negative to positive, and the positive value of Ga1 increased significantly, indicating that the O atom interacts with Ga1 and As1, and the charges of the O atom are transferred to Ga1 and As1 at the same time. When one As-O-Ga bond from the O atom, Ga1 atom and As1 atom is formed, as shown in Fig. 5(d), the Mulliken charge population distribution of this model are quite consistent with that of the model shown in Fig. 5(c), indicating that the O atom located at this position is indeed easy to form bonds with Ga1 and As1, and the formed As-O-Ga oxide is very stable. If one additional Cs atom marked as Cs2 is added above the O atom as shown in Fig. 5(e), the positive charges of Ga1 and As1 decrease evidently, while the positive charges of Ga2, Ga3, and Ga4 increase, and the negative charges of As2 and As3 also increase. This variation in Mulliken charge population indicates that the newly added Cs2 atom reduces the interaction among O, Ga1, and As1 and further reduces the charge transfer caused by oxidation. Meanwhile, the Cs2 atom can cause the charge population redistribution of other Ga/As atoms and Cs1 atom, leading to the new charge transfer between atoms. If there is no O atom adsorbed on the surface as shown in Fig. 5(f), the As atoms in the top As dimer get more negative charge population, which means that the charge transfer increases between Cs1 atom and As atoms in the

top As dimers. The top and side views of Cs-O adsorption sites after geometry optimization on the GaAs(100)- $\beta_2(2 \times 4)$  reconstruction surface are shown in Fig. S3 in the [supplementary material](#). As presented in Figs. S3(e) and S3(f) in the [supplementary material](#), when two Cs atoms are adsorbed, the position of Cs1 atom changes greatly and is far away from the original position because of the repulsion between two Cs atoms. When one O atom is below the Cs1 atom, the O atom can restrain the separation of Cs1 atom and the Cs2 atom can reduce the interaction among O, Ga1, and As1. In contrast to the 2Cs-O adsorption model with the oxidation effect, the 2Cs adsorption model has a lower work function due to its stronger  $\text{Cs}^+-\text{As}^-$  dipoles. Therefore, the excessive Cs and non-excessive O are beneficial to the form of effective dipoles.

For the Cs-O alternating activation recipe with non-excessive Cs supply and excessive O supply, effective dipoles can be constituted to reduce the work function at the beginning through the interaction between O atoms and Cs atoms. However, in this activation process, more O atoms will easily interact with surface Ga atoms and As atoms, especially interact with As atoms in the top As dimer and Ga atoms with dangling bonds to form As-O-Ga oxides, which construct the surface barrier that hinder the escape of photoelectrons. The As-O-Ga oxides are disadvantageous to the reduction of the work function and the formation of  $\text{Cs}^+-\text{As}^-$  dipoles consisting of Cs atoms and the top As dimers. In the subsequent Cs-O alternation process, only when the O flux is stopped and the Cs flux is introduced alone, the newly added Cs atoms can reduce the interaction between O atoms and surface Ga/As atoms and generate new charge transfer, so as to eliminate the inhibitory effect of oxides on the reduction of the work function. While for the Cs-O alternating activation recipe with excessive Cs supply and non-excessive O supply, the increased coverage of Cs atoms can reduce the probability of O atoms directly bonding with Ga atoms and As atoms. Meanwhile, the adsorption probability of O atoms is also improved with the increased coverage of Cs atoms on the surface, which allows more O atoms to be adsorbed on the GaAs surface.<sup>30</sup> Due to the catalysis effect of surface Cs atoms,  $\text{O}_2$  molecules are easily dissociated into O atoms, and O atoms are smaller

in size and thus can enter into Cs atoms easily. The migrated O atoms will cause Cs atoms to dissociate again,<sup>31</sup> which helps to form more  $\text{Cs}^+-\text{O}^{2-}-\text{Cs}^+$  dipoles and further reduce the surface work function. Furthermore, as for the Cs–O alternating activation recipe with completely excessive Cs supply and non-excessive O supply, the increment of photocurrent peak after the first O introduction can be larger. In addition, each alternation cycle can maximize the interaction of more O atoms with more Cs atoms to form dipoles and reduce the charge transfer probability between As dimers and O atoms to avoid the appearance of As–O–Ga oxides as much as possible. From the photocurrent changes in activation experiments C and D, it is seen that the continuous Cs supply can further reduce the Cs–O alternating cycles compared to the intermittent Cs supply, which indicates that more  $\text{Cs}^+-\text{O}^{2-}-\text{Cs}^+$  dipoles are formed in each alternating cycle of activation experiment D. Therefore, in order to improve the photoemission performance of GaAs cathodes, the direct interaction between As atoms in the top As dimers and adsorbed O atoms should be avoided to form As–O–Ga oxides. In this way, more  $\text{Cs}^+-\text{As}^-$  dipoles along with  $\text{Cs}^+-\text{O}^{2-}-\text{Cs}^+$  dipoles can be formed during the Cs–O activation process.

Finally, it should be pointed out that, we only consider the Cs adsorption and Cs–O adsorption nearby the top As dimer and the adjacent Ga atom with the dangling bond in the second layer. In fact, the cases regarding Cs and Cs–O adsorption are complicated because of the numerous adsorption sites and increased adatom coverage. In recent work by Karkare *et al.*,<sup>32</sup> Cs adsorption on the Ga-terminated GaAs(100)-(4 × 2) reconstructed surface was investigated by DFT, and the calculated work function reduction with the change in the Cs surface density is different from our results, which could be ascribed to the different reconstructed surface and adsorption site. As we know, different adsorption sites including T2, T2', T3, T3', T4, T4', D, D', and H on the GaAs(100)- $\beta_2(2 \times 4)$  surface have a significant impact on surface work function and adsorption energy.<sup>24,25</sup> Moreover, the annealing temperature can affect the variation of reconstructed phases on the GaAs(100) surface.<sup>21,26</sup> In addition to the As-terminated  $\beta_2(2 \times 4)$  surface, some other As-terminated GaAs(100) reconstructed phases such as  $\alpha(2 \times 4)$ ,  $\alpha_2(2 \times 4)$ ,  $\beta(2 \times 4)$ , and  $\beta_3(2 \times 4)$ , and Ga-terminated GaAs(100) reconstructed phases such as  $\alpha(4 \times 2)$ ,  $\alpha_2(4 \times 2)$ ,  $\beta(4 \times 2)$ ,  $\beta_2(4 \times 2)$ ,  $\beta_3(4 \times 2)$  can be also modeled to investigate the effect of Cs–O adsorption on GaAs surface activation.<sup>33</sup>

## V. CONCLUSION

Based on the current-driven solid Cs dispensers and O dispensers, different Cs–O activation recipes of p-type GaAs(100) photocathodes were investigated. By comparing differences in photocurrent, quantum efficiency curve, and photocurrent decay among samples using different activation recipes, the effect of excessive Cs supply and O supply on photoemission performance of GaAs photocathodes were clarified by experiments. In combination with density functional calculations and dipole layer model, Cs–O adsorption on the GaAs(100)- $\beta_2(2 \times 4)$  surface was studied theoretically, and the effects of excessive Cs and O on this reconstructed surface were qualitatively analyzed. The results indicate that the activation recipe adopting continuous and completely

excessive Cs supply along with intermittent and non-excessive O supply can obtain higher long-wave response capability and better emission stability. More importantly, the properties of less alternating cycles and easier operation will provide a technical way for realizing the computer-controlled automatic activation of high-performance GaAs photocathodes.

## SUPPLEMENTARY MATERIAL

See the [supplementary material](#) for the changes of vacuum pressure in the Cs–O activation process and in the decay process for the four GaAs cathode samples shown in Figs. S1 and S2, respectively. The top and side views of Cs–O adsorption sites on the GaAs(100)- $\beta_2(2 \times 4)$  reconstruction surface after geometry optimization are presented in Fig. S3.

## ACKNOWLEDGMENTS

The project was supported by the National Natural Science Foundation of China (NNSFC) (Grant Nos. 61771245 and 61301023) and the Science and Technology on Low-Light-Level Night Vision Laboratory Foundation of China (Grant No. J20150702).

## DATA AVAILABILITY

The data that support the findings of this study are available from the corresponding author upon reasonable request.

## REFERENCES

- <sup>1</sup>K. Chrzanowski, *Opto-Electron. Rev.* **21**, 153–181 (2015).
- <sup>2</sup>S. Karkare, L. Boulet, L. Cultrera, B. Dunham, X. Liu, and W. Schaff, *Phys. Rev. Lett.* **112**, 097601 (2014).
- <sup>3</sup>H. Morishita, T. Ohshima, M. Kuwahara, Y. Ose, and T. Agemura, *J. Appl. Phys.* **127**, 164902 (2020).
- <sup>4</sup>P. Schindler, D. C. Riley, I. Bargatin, K. Sahasrabudhe, J. W. Schwede, S. Sun, P. Pianetta, Z. X. Shen, R. T. Howe, and N. A. Melosh, *ACS Energy Lett.* **4**, 2436–2443 (2019).
- <sup>5</sup>J. K. Bae, A. Galdi, L. Cultrera, F. Ikponmwen, J. Maxson, and I. Bazarov, *J. Appl. Phys.* **127**, 124901 (2020).
- <sup>6</sup>J. K. Bae, L. Cultrera, P. DiGiacomo, and I. Bazarov, *Appl. Phys. Lett.* **112**, 154101 (2018).
- <sup>7</sup>C. Feng, Y. J. Zhang, Y. S. Qian, J. Liu, J. Z. Zhang, F. Shi, and X. F. Bai, *Ultramicroscopy* **202**, 128–132 (2019).
- <sup>8</sup>N. Chanlek, J. D. Herbert, R. M. Jones, L. B. Jones, K. J. Middleman, and B. L. Milityn, *J. Phys. D Appl. Phys.* **48**, 375102 (2015).
- <sup>9</sup>T. Guo, *J. Vac. Sci. Technol. A* **7**, 1563–1567 (1989).
- <sup>10</sup>X. Jin, A. A. C. Cotta, G. Chen, A. T. N'Diaye, A. K. Schmid, and N. Yamamoto, *J. Appl. Phys.* **116**, 174509 (2014).
- <sup>11</sup>Y. J. Zhang, Y. S. Qian, C. Feng, F. Shi, H. C. Cheng, J. J. Zou, J. Z. Zhang, and X. Zhang, *Opt. Mater. Express* **7**, 3456–3465 (2017).
- <sup>12</sup>S. Pastuszka, A. S. Terekhov, and A. Wolf, *Appl. Surf. Sci.* **99**, 361–365 (1996).
- <sup>13</sup>D. T. Pierce, R. J. Celotta, G. C. Wang, W. N. Unertl, A. Galejs, C. E. Kuyatt, and S. R. Mielczarek, *Rev. Sci. Instrum.* **51**, 478–499 (1980).
- <sup>14</sup>N. Takahashi, S. I. Tanaka, M. Ichikawa, Y. Q. Cai, and M. Kamada, *J. Phys. Soc. Jpn.* **66**, 2798–2804 (1997).
- <sup>15</sup>L. I. Antonova and V. P. Denisov, *Appl. Surf. Sci.* **111**, 237–240 (1997).
- <sup>16</sup>Z. Miao, F. Shi, H. Cheng, S. Wang, X. Zhang, Y. Yuan, and C. Chen, *Proc. SPIE* **9522**, 95220H (2015).
- <sup>17</sup>K. Togawa, T. Nakanishi, T. Bada, F. Furuta, H. Horinaka, T. Ida, Y. Kurihara, H. Matsumoto, T. Matsuyama, M. Mizuta, S. Okumi, T. Omori, C. Suzuki,

- Y. Takeuchi, K. Wada, and M. Yoshioka, *Nucl. Instrum. Methods Phys. Res. A* **414**, 431–445 (1998).
- <sup>18</sup>N. Chanlek, J. D. Herbert, R. M. Jones, L. B. Jones, K. J. Middleman, and B. L. Militsyn, *J. Phys. D Appl. Phys.* **47**, 055110 (2014).
- <sup>19</sup>Y. J. Zhang, B. K. Chang, J. Niu, J. Zhao, J. J. Zou, F. Shi, and H. C. Cheng, *Appl. Phys. Lett.* **99**, 101104 (2011).
- <sup>20</sup>C. Feng, Y. J. Zhang, J. Liu, Y. S. Qian, J. Z. Zhang, J. Zhao, F. Shi, and X. F. Bai, *Mater. Sci. Semicond. Process.* **91**, 41–46 (2019).
- <sup>21</sup>O. E. Tereshchenko, S. I. Chikichev, and A. S. Terekhov, *J. Vac. Sci. Technol. A* **17**, 2655–2662 (1999).
- <sup>22</sup>T. Nishitani, M. Tabuchi, H. Amano, T. Maekawa, M. Kuwahara, and T. Meguro, *J. Vac. Sci. Technol. B* **32**, 06F901 (2014).
- <sup>23</sup>C. Y. Su, W. E. Spicer, and I. Lindau, *J. Appl. Phys.* **54**, 1413–1422 (1983).
- <sup>24</sup>C. Hogan, D. Paget, Y. Garreau, M. Sauvage, G. Onida, L. Reining, P. Chiaradia, and V. Corradini, *Phys. Rev. B* **68**, 205313 (2003).
- <sup>25</sup>S. E. Kul'kova, S. V. Eremeev, A. V. Postnikov, and I. R. Shein, *J. Exp. Theor. Phys.* **104**, 590–601 (2007).
- <sup>26</sup>O. E. Tereshchenko, D. Paget, P. Chiaradia, F. Wiame, and A. Taleb-Ibrahimi, *Phys. Rev. B* **81**, 035304 (2010).
- <sup>27</sup>W. Wang, G. Lee, M. Huang, R. M. Wallace, and K. Cho, *Microelectron. Eng.* **88**, 3419–3423 (2011).
- <sup>28</sup>M. Scarrozza, G. Pourtois, M. Houssa, M. Heyns, and A. Stesmans, *Phys. Rev. B* **85**, 195307 (2012).
- <sup>29</sup>J. E. Northrup and S. Froyen, *Phys. Rev. B* **50**, 2015–2018 (1994).
- <sup>30</sup>K. V. Toropetsky, O. E. Tereshchenko, and A. S. Terekhov, *JETP Lett.* **88**, 520–523 (2008).
- <sup>31</sup>M. Kamaratos, *Appl. Surf. Sci.* **185**, 66–71 (2001).
- <sup>32</sup>S. Karkare, L. Boulet, A. Singh, R. Hennig, and I. Bazarov, *Phys. Rev. B* **91**, 035408 (2015).
- <sup>33</sup>A. Ohtake, *Surf. Sci. Rep.* **63**, 295–327 (2008).